Chapter 3

# Advances in AFM Imaging Applications for Characterizing the Biophysical Properties of Amyloid Fibrils

Wonseok Lee, Hyungbeen Lee, Gyudo Lee and Dae Sung Yoon

Additional information is available at the end of the chapter

http://dx.doi.org/10.5772/63316

**Abstract**

Although the formation mechanism of amyloid fibrils in bodies is still debated, it has recently been reported how amyloid fibrils can be formed in vitro. Accordingly, we have gained a better understanding of the self-assembly mechanism and intrinsic properties of amyloid fibrils. Because the structure of amyloid fibrils consists of nanoscaled insoluble strands (a few nanometers in diameter and micrometers long), a special tool is needed to study amyloid fibrils at length. Atomic force microscopy (AFM) is supposed to be a versatile toolkit to probe such a tiny biomolecule. The physical/chemical properties of amyloid fibrils have been explored by AFM. In particular, AFM enables the visualization of amyloid fibrillation with different incubation times as well as the concentrations of the formed amyloid fibrils as affected by fibril diameters and lengths. Very recently, the minute structural changes and/or electrical properties of amyloid fibrils have been made by using advanced AFM techniques including dynamic liquid AFM, PeakForce QNM (quantitative nanomechanical mapping), and Kelvin probe force microscopy (KPFM). Herein, we summarize the biophysical properties of amyloid fibrils that are newly discovered with the help of those advanced AFM techniques and suggest our perspectives and future directions for the study of amyloid fibrils.

**Keywords:** amyloid fibril, biophysical property, atomic force microscopy (AFM), Kelvin probe force microscopy (KPFM), PeakForce QNM (quantitative nanomechanical mapping)

## 1. Introduction

Proteins and peptides can be transformed under some physiological conditions from their soluble forms into highly ordered fibrous aggregates, which are called "amyloid fibrils" [1–3]. Amyloid fibrils can be deposited in the tissues and organs in the human body, resulting in the generation of degenerative diseases such as Alzheimer's, Parkinson's, Creutzfeldt-Jakob's, and Huntington's diseases depending on specific sequences of proteins or peptides [4, 5]. On the other hand, the amyloid fibrils have often been exploited for functional roles (e.g., extracellular matrix) by living creatures [6–8]. These amyloid fibrils, commonly known as functional amyloid, are found in bacteria, fungi, insects, invertebrates, and humans. Because of their unique mechanical and biological properties, amyloid fibrils had been used in a variety of organisms as a bacterial coatings, scaffolds, biofilm, information storage and transfer, natural adhesives, and structures for the storage of peptide hormones [7–11]. Although the precise formation mechanism of amyloid fibrils and their pathological/functional behaviors in bodies are still controversial, it has been reported how amyloid fibrils can be formed in vitro, allowing us to understand the fibrillation mechanism and/or the intrinsic properties of the fibrils [12]. Because these fibrils have a distinctive structure that consists of β-sheets that are perpendicularly stacked in thousands of units, aggregating to a few nanometers in diameter and several micrometers in length, a special tool is required to study the conformational (structural) changes of amyloid fibrils in various microenvironments. To investigate the structural changes of amyloid fibrils, many technical tools such as fluorescence microscopy with Congo red and thioflavin-T, transmission electron microscopy (TEM), X-ray diffraction, and nuclear magnetic resonance (NMR) have been used [13, 14]. Recently, atomic force microscopy (AFM) is a good candidate for characterizing such a thin fibrous material *via* high-resolution imaging of the molecular structure and interactions. A sharp stylus mounted at the end of a flexible cantilever is used to probe the amyloid fibrils placed on a piezoelectric scanner which controls the cantilever on the sample in the horizontal ($x$ and $y$) and vertical ($z$) axis (**Figure 1**). The deflection of the cantilever as a result of the interactions (such as van der Waals forces, capillary forces, chemical bonding, and electrostatic forces) between the tip and the sample on substrate is converted into a laser beam reflected on the back of the cantilever. In this system, laser light from diode reflects off the back of the cantilever, and it is recorded as the amplified signal by a position-sensitive detector (PSD), which reconstructs the molecular structure or interactions of amyloid fibrils. AFM has its advantages, for example, the convenience to prepare a sample, working at room temperature and atmospheric pressure, and high-resolution imaging at the single-molecule level, allowing for measuring the physical/chemical properties of amyloid fibrils. In particular, AFM enables scanning to follow the morphological changes of amyloid fibrils in liquid environments, which is powerful as it permits us to visualize amyloid fibrillation under physiological conditions [15]. Recent in vitro studies of amyloid fibrils have demonstrated time-lapse AFM imaging of amyloid fibrillation with different incubation times and concentrations under physiological conditions [16]. Much more recently, AFM application techniques that lie beyond its primary function (i.e., high-resolution imaging) have shown that abundant information of amyloid fibrils can now be accessible. For instance, PeakForce QNM (quantitative nanomechanical mapping) and KPFM (Kelvin probe force microscopy) are, respectively,

http://dx.doi.org/10.5772/63316

beginning to be used to map mechanical properties and to measure the surface charge of amyloid fibrils. Consequently, some unprecedented characteristics (e.g., minute structural changes and/or electrical properties) of amyloid fibrils have been investigated, providing a better understanding of amyloid fibrils [17–23]. In this chapter, we introduce the advanced AFM application methods (i.e., dynamic liquid AFM, PeakForce QNM, and KPFM) for measuring amyloid fibril's features that could not be accessed by conventional AFM technique and summarize the newly discovered biophysical properties of amyloid fibrils with the advanced AFM techniques and suggest our perspectives and future directions for characterizing amyloid fibrils.

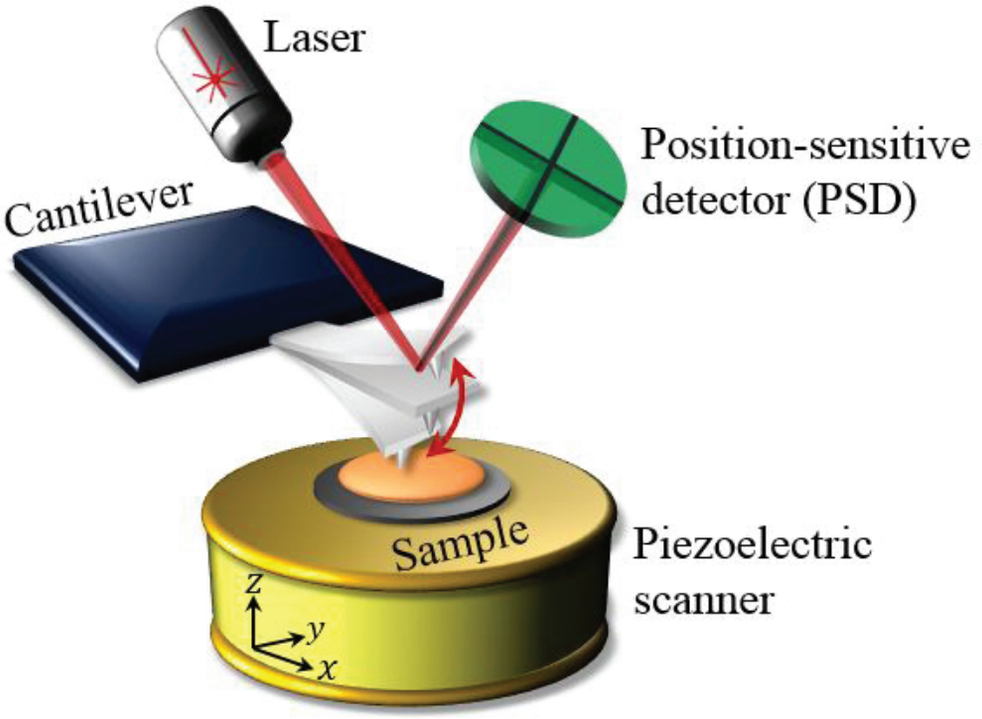


**Figure 1.** Schematic diagram of the principle of AFM.

## 2. Imaging of self-assembled amyloid fibrils in liquid environments

Amyloid fibrils are protein aggregates arising from misfolded proteins, transformed to β-sheet-rich and insoluble fibrils, which can be tangled and deposited in tissues and organs [2]. Characterizing the structure of amyloid fibrils can provide some critical clues about the mechanism of fibrogenesis and accordingly the pathological/functional roles of the fibrils. So far a variety of instruments (e.g., light, X-ray scattering, and NMR) [24, 25] and microscopic methods (e.g., fluorescence microscopy with Congo red and thioflavin-T [26, 27], TEM, and scanning electron microscopy (SEM) [14]) had been used to explore the structure of amyloid fibrils. Although many research results about the structure of amyloid fibrils had been reported by using those tools and/or methods, a fully comprehensive investigation of the self-assembly behavior and structure of various amyloid fibrils has not yet been conducted. AFM

provides additional capabilities and advantages relative to other microscopic methods. For example, it can directly show and measure the structure of an individual fibril. In addition, it is easy to prepare a sample and to get high-resolution imaging at the single-molecule level, allowing for measuring the physical/chemical properties of amyloid fibrils. Furthermore, AFM can scan the conformational changes of amyloid fibrils in a liquid environment, which is powerful to visualize and measure amyloid fibrillation under physiological conditions.

### 2.1. Conventional AFM imaging techniques for amyloid fibrils

Since AFM was invented in the 1980s, it has widely been used as a versatile tool for direct imaging of nano/biomolecules and measuring molecular interactions at the single-molecule level [28–33]. In amyloid research, it has been reported that AFM is used to elucidate the fibril formation mechanism and to monitor kinetics and morphology of amyloid fibrils such as α-synuclein, insulin, and the B1 domain of protein G, a base model for immunoglobulin light-chain variable domains related with fibrils [34]. For AFM imaging, the fibrils were deposited on a freshly cleaved mica substrate. AFM images were collected in air under ambient conditions at a scan frequency of 1–2 Hz. From the analysis of AFM images, all fibrils (α-synuclein, insulin, and the B1 domain of protein G) are in correspondence with the general hierarchical assembly model, like amyloid-β (Aβ; 1–40 and 1–42), with which mature amyloid fibrils are formed by the intertwining of protofibrils. When first aggregated into protofibrils, the measured heights (i.e., fibril diameters) range from 1.2 to 3.5 nm. The structural information of the fibrils such as the fibril diameter and contour length depends on the protein species. Several protofibrils can pack together to form a mature fibril (5.2 ± 0.3 nm in height).

It has been reported that different stages of amyloid aggregation (i.e., hierarchy) can be examined by conducting a statistical analysis of acquired high-resolution AFM images [35]. β-Lactoglobulin (β-lg) fibrils are synthesized in vitro by heat denaturation at pH 2. It was shown that the β-lg amyloid-like fibrils are considered to be a semiflexible fibril structure (**Figure 2**). This means that the globular proteins (β-lg monomer) can be transformed into semiflexible fibrillary structures. The average height and contour length of β-lg fibrils were precisely measured by performing a statistical analysis on the AFM images. Each fibril has contour lengths in the range of 50 nm to 10 μm with a persistence length ranging from 16 nm to 1.6 μm. These distinct structural information of fibrils make them ideal model systems for the study of semiflexible polymers [36]. In that study, valuable structural information concerning individual fibrils in AFM images was produced, such as splitting or thinning of fibrils and even periodic height fluctuations of the fibrils. The periodic fluctuations in height provide a highly important clue about the packing of the protofibrils to form mature fibrils. **Figure 2** presents AFM images of fibrils with four different periods ranging from 35 to 135 nm, corresponding to average heights of fibrils ranging from 4 to 10 nm, respectively. Thus, the periodicity is found to increase linearly with the height of the fibrils. These hierarchical structures of β-lg fibrils can be represented from single to five-stranded packed twisted ribbon, helix-like structures, which can be compared with dynamic simulations using a coarse-grain molecular model.

http://dx.doi.org/10.5772/63316

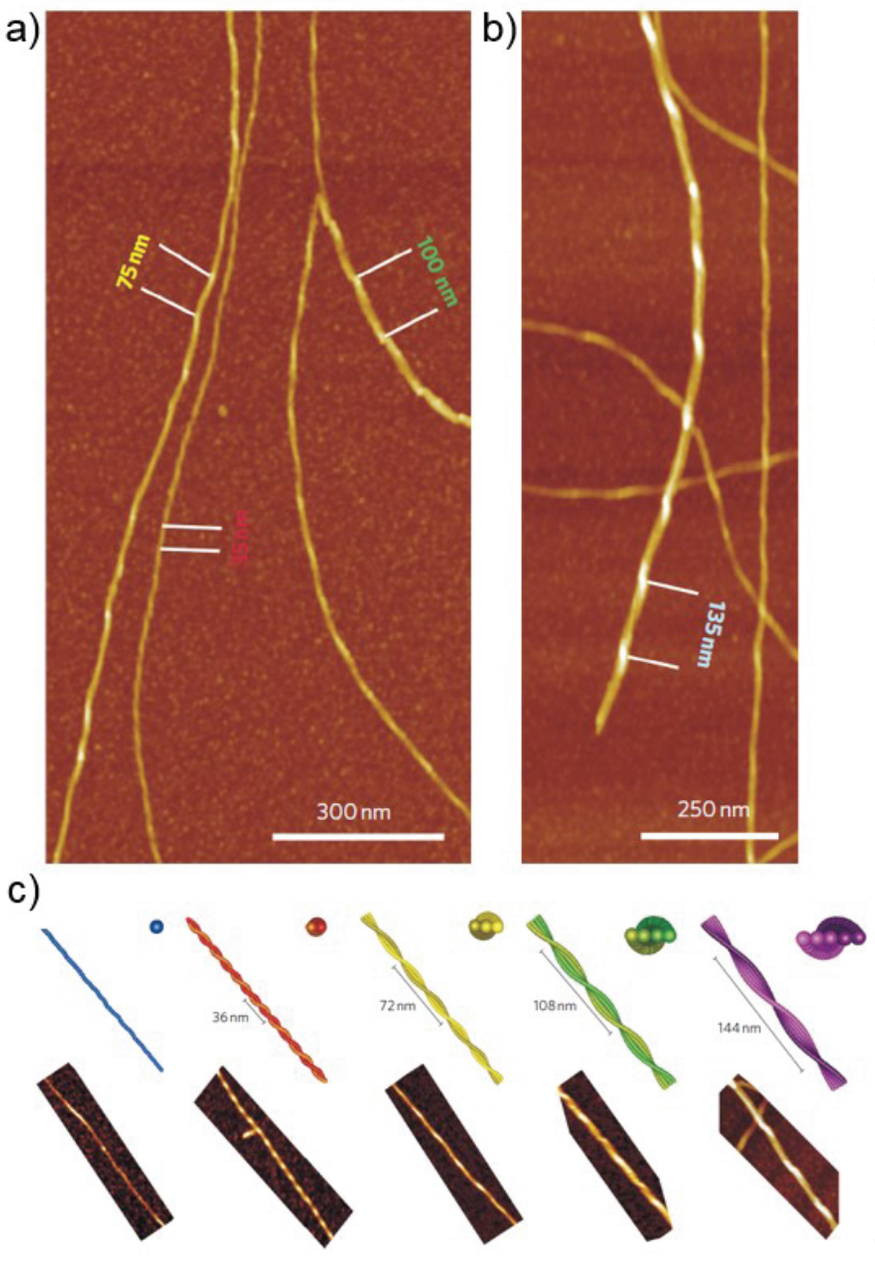


**Figure 2.** Different periods of β-lactoglobulin fibrils. (a) AFM height image of fibrils with a period of 35 nm (for fibrils with a maximum height of 4 nm), 75 nm (maximum height, 6 nm), and 100 nm (maximum height, 8 nm). (b) Example of a fibril with a period of 135 nm and a maximum height of 10 nm. (c) AFM images and corresponding coarse-grain molecular dynamics reconstructions of left-handed helical fibril formation from the twisting of multistranded ribbons, with the number of filaments ranging between 1 and 5. Figures reproduced with permission from Ref. [35], © 2010 NPG.

It is highly important to study initial fibrillation of amyloid proteins for developing an inhibition method for amyloid fibrils and plaques. Although attempts with many conventional methods such as fluorescent assays with dye and optical spectroscopy had been reported, insight into the mechanisms of formation of initial fibrils at the molecular level has yet to provide clarity. To address that issue, AFM techniques can investigate growing fibrils in

greater detail. **Figure 3** shows topological images of the β-lg fibrils acquired after 30 and 45 min incubation [37]. As the incubation time was increased, the contour length of fibrils increased in the range from 520 to 860 nm. The two-filament packed structure was only observed after a heating time of 30 min. But after a heating time of 45 min, fibrils of more than two filaments were observed. From those results, AFM analysis can provide us with some significant structural information not only topological images but also details such as height, contour length, and periodicity from fluctuations along the fibril length. In addition, it can show the formation characteristics of amyloid fibrils, including the critical steps driven by nucleation and growth of individual fibrils. These findings from the use of AFM imaging may help researchers gain understanding of the origin of fibrils and may assist with the development of therapeutic treatments for degenerative diseases that are generated by many different amyloidogenic proteins.

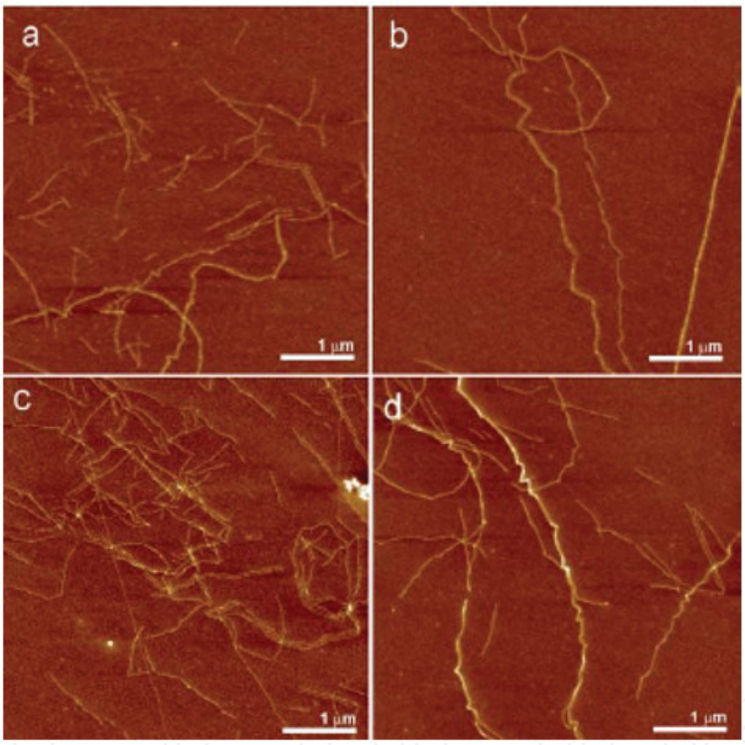


**Figure 3.** AFM height images of heated β-lactoglobulin at pH 2 and 90°C for the heating time of (a and b) 30 min and (c and d) 45 min. Figures reproduced with permission from Ref. [37], © 2011 The Royal Society of Chemistry.

### 2.2. Advantages of AFM imaging of amyloid fibrils in liquid environments

As we mentioned above, AFM imaging of amyloid fibrils is strong advantageous not only in the characterization of the structure of amyloid fibrils but also for the observation of initial fibrillation of amyloidogenic proteins. These investigations of amyloid fibrils in ambient atmospheric conditions by AFM imaging yield the basic understandings of the characteristics of amyloid fibrils, but all of these processes (such as fibrillation and conformation changes) actually take place in a liquid environment (i.e., in human body fluid). In addition, the

http://dx.doi.org/10.5772/63316

formation of amyloid fibrils continuously occurs in the human body, not discretely, which is why liquid AFM is particularly important to more precisely and continuously observe to fibrils in comparing with conventional AFM.

In the research field of amyloid fibril, real-time monitoring of fibril growth is necessary to investigate the mechanism of amyloid fibril formation. It has been reported that the direct observation of fibrillation of Aβ peptide on different substrates is achieved by using in situ AFM analysis in a liquid environment [15]. They used two types of substrate: hydrophilic mica and hydrophobic graphite. Hydrophilic mica can be considered a model of the hydrophilic components of cell membranes such as anionic phospholipids. The hydrophobic graphite may be used as a model of hydrophobic elements of cell membrane (e.g., lipid bilayers and lipoprotein particles), in which elements Aβ peptide can localize in both plasma and cerebrospinal fluid in vivo. An in situ AFM study of Aβ fibril aggregation was followed by continuous imaging in phosphate-buffered saline (pH 7.4, protein concentration 10–500 mM). Aβ peptides initially were formed with pseudomicellar aggregates and then tend to form linear structures, such as protofibrils, as the Aβ concentration was increased on the hydrophilic mica substrate. However, Aβ peptides were formed with elongated sheets structures on the hydrophobic graphite substrate. This difference by substrates is the distinguishable characteristics between β-sheets and $\alpha$-helices. These studies show that an in situ AFM study is able to directly observe not only the amyloid aggregation in physiological fluids but also fibrillation driven by interactions at the interface of hydrophilic and hydrophobic substrates. It may be helpful to understand the mechanism of formation of Aβ fibrils in membranes and lipoprotein particles in vivo.

AFM has been employed not only to study the formation of amyloid fibrils in vitro but also to investigate ex vivo amyloid material isolated from organs, specifically hearts, of patients. The AFM analysis of natural amyloid fibrils produced by the Leu174Ser apolipoprotein A-I variant (ApoA-I-LS) has been reported. ApoA-I-LS amyloid fibrils were obtained from two different patients, and conformational changes of the fibrils in both air and liquid environments were measured [38]. The fibrils from both patients were identified by small-angle X-ray diffraction patterns, indicative of residual $\alpha$-helical structure. In a liquid environment, it was observed that amyloid fibrils show poor adhesion properties on a mica substrate. But, from acquired AFM images, it was found that globular aggregates were easily adsorbed on mica. These results revealed the existence of fibrils as well as pre-fibrillar aggregates, with common morphologies and compatible sizes of fibrils and globules for both patients.

In addition, AFM imaging in a liquid environment is able to reveal unique and intrinsic properties of amyloid fibrils, which cannot be seen by any other method. It has been reported that the conformations of C-terminal tails outside of the $\alpha$-synuclein amyloid fibrils are variable depending on environmental conditions by using structural information from liquid AFM imaging, as in **Figure 4** [39]. They suggested that the exposed C-terminus is unstructured and looks like a polymer bush and that the strongly negatively charged C-terminus has various functions and conformations with different ion concentrations (i.e., in the range of 0–5 M NaCl). It was also observed that the height of $\alpha$-synuclein fibrils imaged in air appears to be about 17% lower than those of the same fibrils imaged in a liquid environment. This

phenomenon is attributed to the collapse of C-terminus depending on the drying of the fibrils. Measuring the conformational changes of the C-terminus in amyloid fibrils by AFM imaging sheds light on the estimation of the transformation of the exterior structures of amyloid fibrils.

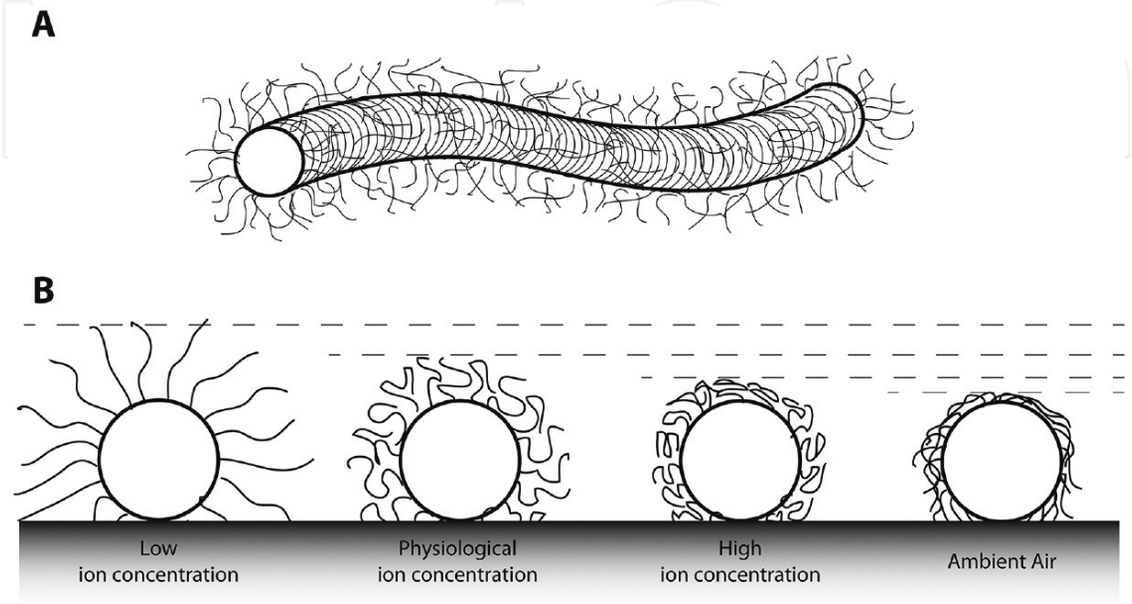


**Figure 4.** (a) Schematic representation of a fibril with stacked β-sheet folded monomers perpendicular to the fibril axis and an unstructured C-terminus outside the fibril. (b) Different conformations of C-terminal tails outside the fibril core in liquid conditions with different ion concentrations and in ambient air. Figure reproduced with permission Ref. [39], © 2012 American Chemical Society.

## 3. PeakForce QNM (quantitative nanomechanical mapping) of amyloid fibrils

Amyloid fibrils have been known as β-sheet-rich structures, which are consisted with dense hydrogen-bonding networks [40]. The self-assembly aggregates can be formed with stackings of several hundreds to thousands of cross β-sheet units, a few nanometers in diameter, and several micrometers in length. Such hierarchical structure of fibrils is highly related to pathological meanings as well as to functional features due to their marvelous mechanical properties, which are comparable to those of silk and/or steel [13, 41]. Characterization of biophysical properties of amyloid fibrils has significant implications ranging from application to medicines and engineering for designing amyloid-based nanomaterials. To measure biophysical properties of amyloid fibrils, although in recent decades many research results had been reported that had been obtained by using various techniques such as optical, magnetic tweezer and dynamic mechanical analysis [13], AFM techniques are commonly used for both manipulation at the single-molecule level and force spectroscopy of nanomaterials

http://dx.doi.org/10.5772/63316

(i.e., amyloid fibrils). Moreover, AFM nanoindentation has been used to study nanomechanics of amyloid fibrils [42].

AFM nanoindentation is performed by mapping force-distance (F-D) curve on the region of interest in the sample [43, 44]. F-D curve measurement is based on the deflection theory of a cantilever beam and the contact mechanics. The degree of nanomechanical deflection of AFM cantilever originated from the physical interactions between the AFM tip and the sample can be converted to the applied forces to the cantilever. When F-D curve records, the cantilever approaches and indents the sample until a certain predefined force is reached, and then the cantilever is retracted. During the approach and retract cycle, the force is continuously measured, which is a F-D curve for one point of the sample (**Figure 5**). The mechanical properties such as Young's modulus, adhesion force, and deformation energies of amyloid fibrils can be determined directly from the recorded data (F-D curve) by AFM nanoindentation. In particular, to extract the accurate Young's modulus of the sample from F-D curves, contact mechanics theory is used. There are three different types of representative contact mechanics models (Hertz, DMT, and JKR) depending on either the type of sample or the structure of AFM tip [18]. The Hertz model presumes a nonadhesive contact between the tip and the sample, while the Derjaguin-Muller-Toporov (DMT) and Johnson-Kendall-Roberts (JKR) models are considered to be adhesive materials. DMT model further includes the extra constant adhesion term, which indicates the adhesive force outside the contact area. The JKR model demonstrates the adhesion forces inside the contact area between the tip and the sample. Those model equations are as follows:

$$\boldsymbol{Hertz}: \boldsymbol{F} = \frac{\mathbf{4}}{\mathbf{3}} \boldsymbol{E}^{*} \ \overline{\boldsymbol{R}} \boldsymbol{\delta}^{\frac{\mathbf{3}}{\mathbf{2}}},$$

$$\boldsymbol{Derjaguin{-}Muller{-}Toporov} \ \ \boldsymbol{DMT} : \boldsymbol{F} = \frac{\mathbf{4}}{\mathbf{3}} \boldsymbol{E}^{*} \ \overline{\boldsymbol{R}} \boldsymbol{\delta}^{\frac{\mathbf{3}}{\mathbf{2}}} - \mathbf{2}\boldsymbol{\pi} \boldsymbol{R} \boldsymbol{\gamma}$$

$$\boldsymbol{Johnson - Kendall - Roberts} \ \ \boldsymbol{JKR} : \ \boldsymbol{F} = \frac{\mathbf{9}}{\mathbf{4}} \boldsymbol{E}^{*} \ \overline{\boldsymbol{R}} \boldsymbol{\delta}^{\frac{\mathbf{3}}{\mathbf{2}}} \cdot \Delta \boldsymbol{\gamma} \boldsymbol{\pi}$$

$$\frac{\mathbf{1}}{\boldsymbol{E}^{*}} = \frac{\mathbf{1} - \boldsymbol{v_m}^{\mathbf{2}}}{\boldsymbol{E_m}} + \frac{\mathbf{1} - \boldsymbol{v_i}^{\mathbf{2}}}{\boldsymbol{E_i}}$$

where $F$ is the force, $\delta$ is the AFM indentation depth (distance), $R$ is the radius of cantilever tip, $E^*$ is the reduced elastic modulus, and $\gamma$ is the work of adhesion. $E^*$ is calculated by the

relationship between the elastic modulus and Poisson ratio of AFM cantilever ($E_i$, $\nu_i$) and sample ($E_m$, $\nu_m$).

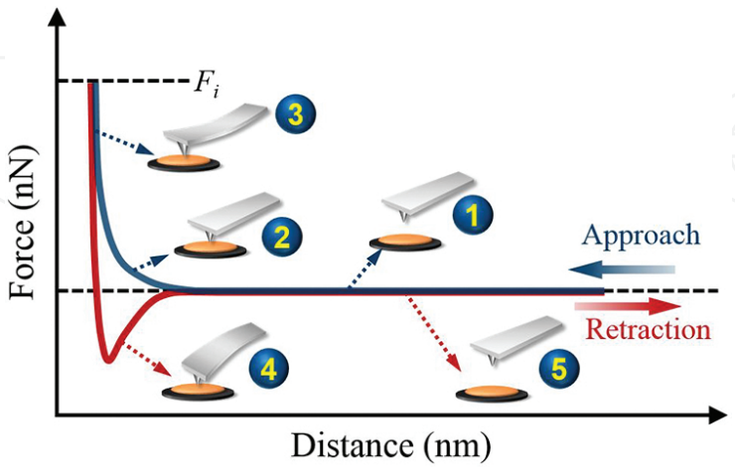


**Figure 5.** The schematic illustration of F-D curve acquisition process during AFM nanoindentation. Approach (blue) and retraction (red) F-D curves. Illustration depicts the cantilever approaching to and retracting from the sample as follows: (1) approaching, (2) initial contact, and (3) repulsive contact. (4) Adhesion and (5) noncontact regimes recorded upon retracting the cantilever and sample.

In recent decades, to measure the physical properties of amyloid fibrils more precisely and quantitatively, PeakForce QNM technique has been developed. PeakForce QNM is a robust F-D curve mapping technique, which is beneficial for soft delicate biological samples. It is able to map and distinguish between nanomechanical features, including the DMT modulus (1 kPa to 100 GPa), adhesion, energy dissipation, and deformation by utilizing PeakForce tapping technology [45, 46]. It can acquire high-resolution topographic images and simultaneously collect a quantitative mapping of the intrinsic mechanical properties of amyloid fibril.

### 3.1. Principle of PeakForce QNM

PeakForce tapping is one of the scanning modes, which is especially suited to applications to the measurement of mechanical properties of biological samples [18]. In this mode, the probe is oscillated at a low frequency (1–2 kHz), while capturing a force-distance curve (F-D curve) plots each time the AFM probe taps on the sample by directly controlling the probe-sample interaction. To describe the details, one cycle of the PeakForce tapping trajectory is shown in **Figure 6a** [17]. During the approach to the sample, the probe begins (A) with a noncontact force (i.e., attractive force) until contact on the sample. The Z piezo presses it downward until the probe contacts the sample (B); the probe continuously presses until the probe reaches the setpoint (i.e., maximum force) (C). The setpoint, which is one of the parameters of the probe-sample interaction, is used during AFM topography. After reaching the peak force at point C, the tip is pulled off the surface at point D, which means maximum adhesion. Finally, the curve levels and the probe tip returns to its original position (E).

http://dx.doi.org/10.5772/63316

Accurate controlling of the probe position and feedback permits calculation of several properties from the F-D curve produced by the direct measurements simultaneously at each pixel in **Figure 6b**. From this curve, the peak force is measured at point C, which is used as the imaging feedback signal. As the probe is scanned over the surface, this signal produces a topological image. Adhesion force is measured at D, which is calculated as the force difference between the baseline and the minimum force value of the curve. Simultaneously, Young's modulus is obtained by fitting the DMT contact mechanics model to the retraction curve (at points C to D). The dissipation information is obtained by integrating the area between the extension and retraction curves and the deformation of the sample is calculated as the distance between the contact point on the adhesion curve and the maximum indentation. This unique technique is called PeakForce QNM. Compared to a typical AFM imaging method, PeakForce QNM can simultaneously yield high-resolution AFM imaging with quantitative mechanical property mapping. PeakForce QNM has recently emerged as a means of measuring the intrinsic and biophysical properties of nanomaterials [47], including amyloid fibrils [17, 19]. The following section will discuss the mapping the mechanical properties of amyloid fibrils by PeakForce QNM.

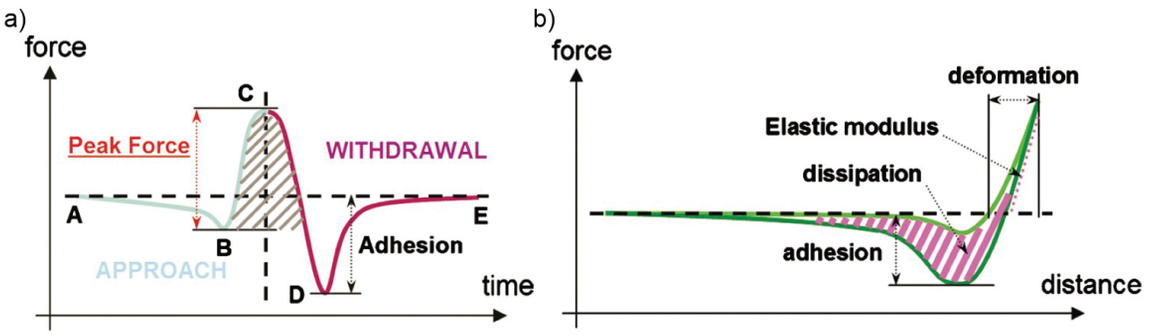


**Figure 6.** Principle of PeakForce QNM operation. (a) One cycle of the PeakForce tapping curve. (b) Calculation of the different peak force channels. Figure reproduced with permission Ref. [17], © 2011 AIP.

### 3.2. Mapping the mechanical properties of amyloid fibrils by PeakForce QNM

In the folding process, synthesized peptide chains can be transformed into three-dimensional protein structure, which has diverse functions in biological organism, through intermolecular interactions such as hydrogen and hydrophobic bonding [3, 48]. The proteins have intrinsic mechanical properties depending on the specific amino acid sequence, lengths, and complex environments. Meanwhile, misfolded proteins, commonly known as "amyloid protein," can be transformed into β-sheet-rich fibrillary structure (i.e., amyloid fibril) during fibrillation process. Amyloid fibrils have tremendous mechanical properties (a few GPa), implying a comparatively high stiffness. Moreover, it displays structural polymorphism, including twisted ribbons, helical ribbons, and nanotube structure [19], which is supposed to show a difference in mechanical properties. Amyloid species (amyloid proteins and fibrils) can be accumulated and deposited in the human body, which is associated with proteoglycans, in particular, heparan sulfate proteoglycans [48, 49]. These findings raise the question

about the underpinning nature of the correlation between the mechanical properties of amyloid fibrils and its pathological roles in living systems as well as the use of fibrils as nanoscale materials.

PeakForce QNM has emerged as mechanical property mapping variant of AFM nanoindentation that had been used for several decades. PeakForce QNM has been used to measure the Young's modulus of β-lg fibrils deposited on mica [17]. It is of importance to measure the mechanical properties of β-lg fibrils because they have been used to make new nanomaterials by mixing with nanoparticles and nanowires for applications in various research fields. Using PeakForce QNM, the average height of the fibrils was measured to be 2.5 ± 0.5 nm and DMT modulus images were concurrently acquired. The Young's modulus of β-lg fibrils was estimated to be 3.7 ± 1.1 GPa. This result from PeakForce QNM analysis is similar to that of a previously reported Young's modulus of insulin fibrils (~3.3 GPa).

Amyloid fibrils can be generally formed with many different proteins such as Aβ (1–42), α-synuclein, albumin, etc., which have pathological and functional meanings. These fibrils often exhibit structural polymorphism due to interweaving of the several protofibrils. It has been demonstrated that amyloid fibrils appear in various structures such as ribbon-like and nanotube-like packed fibrils. PeakForce can precisely measure the Young's moduli of several amyloid fibrils, assembled from α-synuclein, Aβ (1–42), tau protein, insulin, β-lg, lysozyme, ovalbumin, and bovine serum albumin fibrils, as in **Figure 7** [19]. In addition, it demonstrated that PeakForce QNM can provide us some clues regarding structural polymorphism of amyloid fibrils by the exact estimation of Young's modulus. The measured Young's modulus values are twisted ribbon structure, 2.3 ± 0.6 GPa, and helical ribbon and nanotube structures, 2.3 ± 0.7 GPa and 2.4 ± 0.5 GPa, respectively. They also measured the value of Young's modulus for insulin amyloid fibrils (3.2 ± 0.6 GPa), which is very similar to that of a previously study of insulin (3.3 ± 0.4 GPa).

Recently, amyloid fibrils have attracted great attention because of outstanding features based on their mechanical properties as nanomaterials. To investigate the potential of amyloid fibrils as biomaterials, it is important to understand the mechanism of the fibrillation process and to quantify the mechanical properties. By performing the PeakForce QNM technique, the mechanical properties of the Aβ-42 fibrils during the fibrillation process have been measured, as in **Figure 8** [21]. The Young's modulus of the oligomers, protofibrils, and mature Aβ-42 fibrils was evaluated. During fibrillation, in which oligomers grow into protofibrils and then finally formed mature fibrils, the mechanical property (i.e., Young's modulus) increased. Hydrogen bonds between β-sheets may need to be reckoned with when one tries to determine the mechanical properties of amyloid fibrils. The changes in β-sheets in oligomers, protofibrils, and mature fibrils may have effects on the mechanical properties during the fibrillation process. These results could be of great significance for the elucidation of the mechanical properties of amyloid fibrils for the planning of new material strategies.

http://dx.doi.org/10.5772/63316

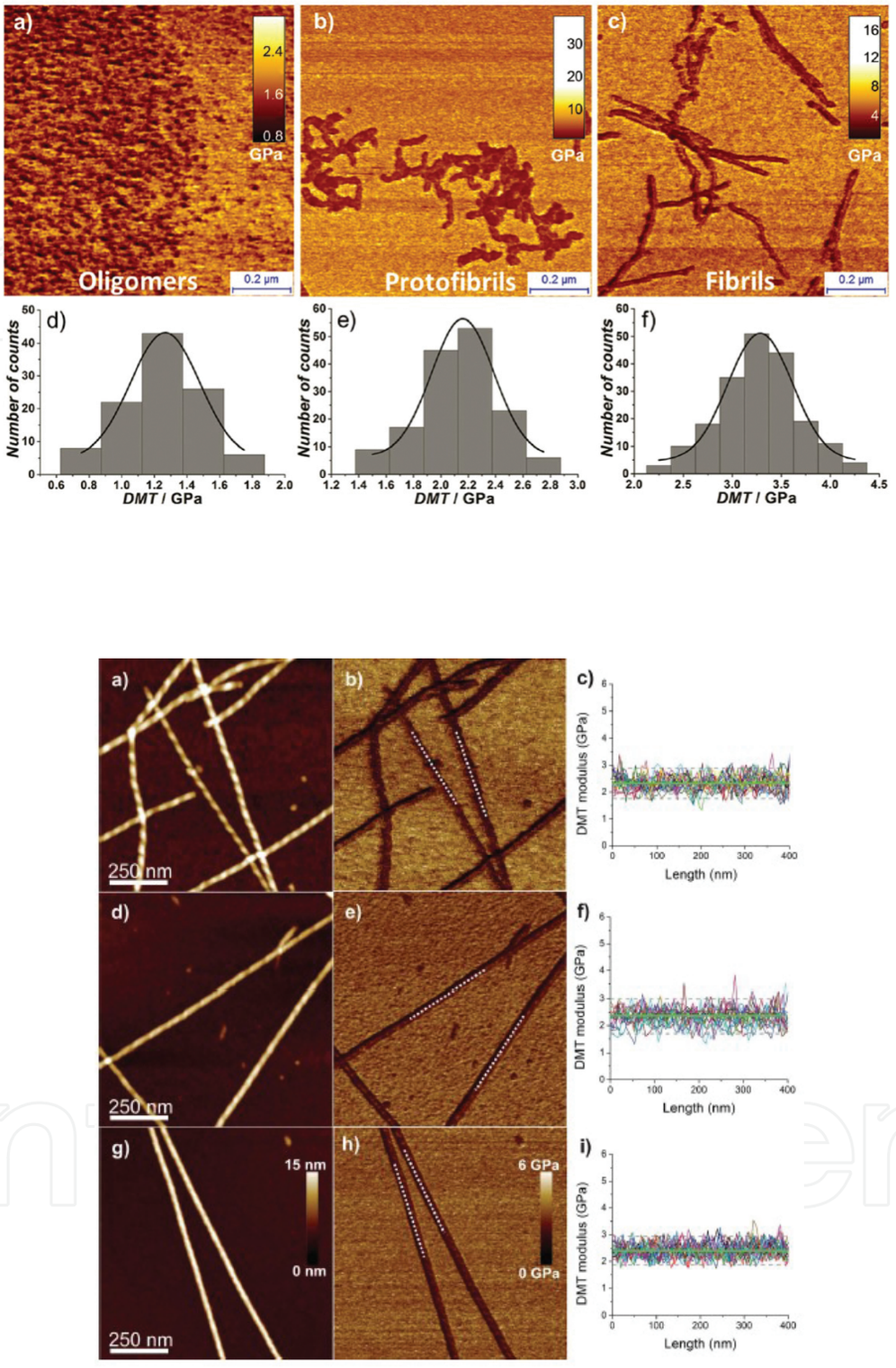


**Figure 7.** AFM height image of (a) twisted ribbon, (d) helical ribbon, and (g) nanotube-like structures of the end-capped heptapeptide $CH_3CONH$-βAβAKLVFF-$CONH_2$. AFM DMT modulus image of (b) twisted ribbon, (e) helical ribbon, and (h) nanotube-like structures. The dashed lines mark the positions at which the DMT modulus was analyzed. Profiles of DMT moduli along (c) twisted ribbon, (f) helical ribbon, and (i) nanotube-like structures. The data were obtained by the analysis of 20 fibrils for each type. Figure reproduced with permission Ref. [19], © 2012 The Royal Society of Chemistry.

**Figure 8.** Evolution of the Young's modulus of Aβ-42 during the fibrillation process. DMT modulus AFM images of oligomers at 0 h (a), protofibrils at 48 h (b), and fibrils at 72 h (c). Distribution of the measured Young's modulus for oligomers (d), protofibrils (e), and fibrils (f). Figure reproduced with permission Ref. [21], © 2015 Wiley-VCH Verlag GmbH & Co. KGaA.

## 4. Kelvin probe force microscopy (KPFM) of amyloid fibrils

The amyloid fibril has been implicated in the various neurodegenerative diseases such as Alzheimer's, Parkinson's, Creutzfeldt-Jakob's, and Huntington's diseases [1–3], but the molecular mechanism of an amyloid toxicity is still debated [49–51]. To address this issue, scientists have investigated different possibilities for molecular behavior of amyloid-forming proteins that are correlated with the amyloid toxicity mechanism [52–54]. The leading proposed mechanism of the amyloid toxicity refers to the electrostatic interactions between the lipid membrane of cells and amyloid oligomers/fibrils (i.e., cytotoxicity) [55–57]. In addition, the electrostatic forces play important roles in the accumulation of proteinaceous aggregates as amyloid plaques or Lewy bodies. Therefore, the measurement of electrical properties of amyloid fibrils offers a new insight into the mechanism of amyloid fibril formation and toxicity.

KPFM has been considered as a powerful instrument for detecting the electrical properties of nano/biomaterials including molecules [58–62] by mapping the surface potential (the work function) of them. KPFM is carried out by a conducting AFM probe, which ascends to lift scan height. While the probe scans a sample surface of interest, a potential offset between the tip and the surface is recorded at each point of the scanned area. Furthermore, a high spatial resolution of KPFM is attributed to highly sharp conducting AFM tip by measuring the local contact potential difference (CPD) between the tip and the sample (**Figure 9**). Accordingly, KPFM has recently been used for characterizing the surface potential of amyloid fibrils [20, 23, 63] to unveil the molecular mechanism governing amyloid fibril formation and toxicities.

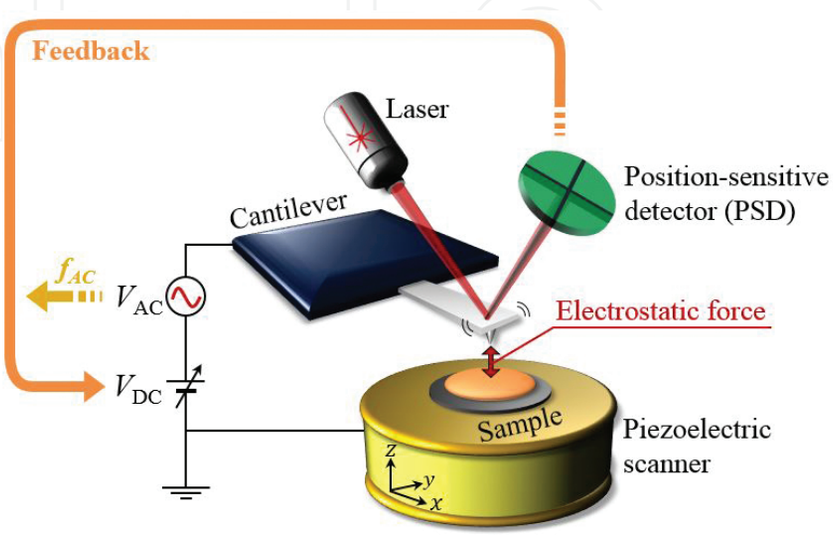

**Figure 9.** A schematic illustration of Kelvin probe force microscopy (KPFM) method for the measurement of electrical properties of material.

### 4.1. Principle of KPFM

In KPFM studies of mapping the surface potential, the surface potential of the materials is measured by the CPD between the material surface and the KPFM conducting cantilever tip, where the CPD is the variation in work function between different surfaces (the material surface and the tip) [58]. The CPD of two materials is determined, depending on their electronic/electrical characteristics. The characterization of the CPD is able to use not only for measuring the work function of metallic material and semiconductor surfaces but also for mapping the surface potential of biomolecules such as various proteins [64], DNA molecules [59, 60], and amyloids [20, 23, 63].

The hardware system of KPFM is founded upon the principle of the Kelvin method, which is a standard measurement method of the determination the CPD [65] (this is a reason why KPFM applies the term "Kelvin"). In the Kelvin probe method, the CPD ($V_{CPD}$) between two different materials is plainly defined as

$$V_{CPD} = \frac{\varphi_1 - \varphi_2}{-e} \tag{1}$$

where $\varphi_1$ and $\varphi_2$ are the work functions of two different materials (in KPFM, $\varphi_1 = \varphi_{tip}$ and $\varphi_2 = \varphi_{sample}$) and $e$ is the charge of an electron. The probe, which consists of material with a known work function, is aligned to the sample surface for forming a capacitor. The reference electrode probe is vibrated, causing a variation in the capacitance between two plates, resulting in an electric current $i(t)$ and the generated current is given by

$$i(t) = V_{CPD}\omega\Delta C\cos\omega t \tag{2}$$

where $\omega$ is the frequency of vibration, $\Delta C$ is the change of capacitance, and $V_{CPD}$ is the contact potential between the probe and the sample surface. $V_{CPD}$ is measured by applying an contrasting external DC (direct current) bias voltage ($V_{DC}$), which is varied until the $i(t)$ is minimized.

The fundamental KPFM system is similar to the Kelvin method [65]. Mapping the surface potential of a material using KPFM, an electrostatic force ($F_{ES}$) *via* the $V_{CPD}$ between a KPFM conducting tip and a material, is caused by an AC (alternating current) voltage $V_{AC}$ with a DC offset bias $V_{DC}$ which is applied between a tip and a material [66]. The $F_{ES}$ between the tip and sample is defined as

$$F_{ES}(x,t) = -\frac{1}{2}\frac{\partial C(x)}{\partial x}\left[\left(V_{DC} \pm V_{CPD}\right) + V_{AC}\sin\omega t\right]^2 \quad (3)$$

where $x$ is the distance between the KFPM conducting tip and a material. The electrical force component with frequency $\omega$ (related to differential value of "($V_{DC}$ ± $V_{CPD}$) $V_{AC}$ sin $\omega t$") is obtained from the PSD) signals through a lock-in amplifier. A feedback controller applies the $V_{DC}$ to the KPFM system until the electrical force component with frequency $\omega$ is minimized. Accordingly, $V_{CPD}$ between a KPFM conducting tip and a material is determined based on altering the DC offset bias $V_{DC}$.

### 4.2. Mapping the surface potential of amyloid fibrils

As mentioned above, the evaluation of electrical properties of amyloid fibrils would offer a better understanding of the mechanism of amyloid fibril formation and toxicity. To date, some of researchers have reported KPFM analysis for quantitative estimation of electrical properties of amyloid fibrils. It has been reported that synthesis of the amyloid-β-(25–35) peptide ($A\beta_{25–35}$) (with sequence GSNKGAIIGLM) fibrils and KPFM analysis of them [67]. Although the major components of neurotic plaque found in AD are 10-to-42-residue-long Aβ peptides ($A\beta_{1–40}$/$A\beta_{1–42}$), shorter fragments of peptides are also involved, such as $A\beta_{25–35}$. It has been reported that $A\beta_{25–35}$ can form readily β-sheet aggregates and is toxic to neurons. The surface potential analysis of $A\beta_{25–35}$ fibrils was performed by KPFM. The samples were prepared for KPFM imaging by depositing the solutions on chemically cleaned silicon (Si) substrates, and KPFM records were made for both the sample topography and the phase shift by using a two-pass method, namely, lift mode KPFM. It was found that the five fibrils have almost the same CPD values, which are about −10~ to −15 mV relative to the Si substrate. By calibrating the work function of cantilever tip, the work function of the $A\beta_{25–35}$ fibril was determined to be about 4.62 eV. However, the main thrust of this study is the surface potential analysis in regards to the interaction of gold nanoparticles (AuNPs) with $A\beta_{25–35}$ peptides, which we shall mention further on.

http://dx.doi.org/10.5772/63316

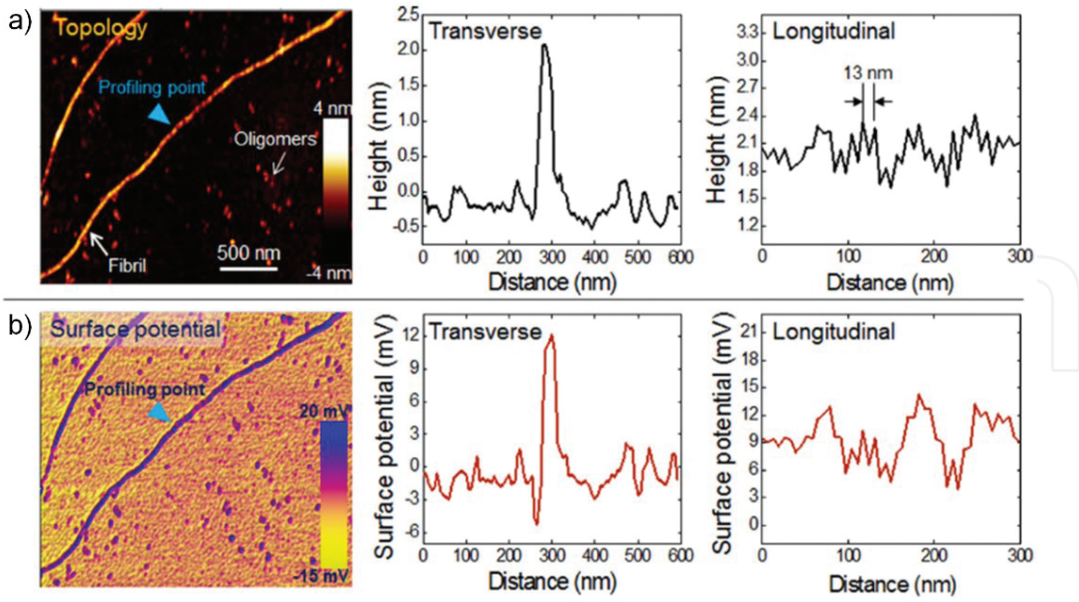


**Figure 10.** AFM and KPFM images of β-lactoglobulin amyloid fibrils. In each image of AFM topography (panel a) and surface potential (panel b), the white arrow shows a single amyloid fibril. A blue arrow indicates the location of amyloid fibril, at which the transverse profile of surface potential and topography were obtained. In the profiles of both topography and surface potential at longitudinal direction. Figures reproduced with permission from Ref. [20], © 2012 AIP.

Recently, β-lg has attracted much interest as an alternative amyloid precursor to be used to investigate the fibrillation mechanism and to fabricate various composites because of its inexpensive price and easy fabrication. The electrical properties of the β-lg fibrils using KPFM have been studied, which was the first attempt to visualize mapping the surface potential distribution of a single amyloid fibril [20]. As shown in **Figure 10**, the surface potential of the fibril is positive (e.g., ~12 mV) since the pH of a buffer solution is lower than the isoelectric point (pI) of β-lg (p*I* ~ 5.0). Interestingly, it is found that the surface potential profile of the fibril is critically dependent on the fibril diameter and periodicity, which implies that the surface charge distribution of amyloid fibril is closely related to its conformation. This report demonstrated that KPFM is able to accurately obtain the surface potential of the amyloid fibrils with their conformational structures. Moreover, KPFM was shown to have the possibility of being usable as a detection platform for peptide identification of amyloid fibrils because KPFM measurement has proven to be powerful enough to detect a delicate difference of the surface potential.

### 4.3. Quantifying the electrical properties of amyloid fibrils in different environments

For understanding electrostatic interactions between various nano/biomaterials and amyloid oligomers/fibrils, or the accumulation of proteinaceous aggregates as amyloid fibrils/plaques, many researchers have reported quantifying the electrical properties of amyloid fibrils in different environments. In recent decades, nanomaterials, especially nanoparticles, have been increasingly applied in biomedicine for therapeutic and diagnostic purposes [68–70]. In

particular, AuNPs have been widely used in the field of chemistry and biomedical science [71–73] due to their electronic [74] and molecular-recognition properties [75]. Due to the properties of AuNP, it has been found that the AuNPs can either promote or inhibit the aggregation of Aβ proteins, depending on the size and functionality of AuNPs or the pH value of the solution. As mentioned above, the surface potential analysis on the interaction of AuNPs with $A\beta_{25–35}$ peptides has been studied [67]. To investigate the effect of AuNPs on fibrillation, $A\beta_{25–35}$ peptides were incubated with AuNPs at room temperature for 5–12 days. KPFM was used to record both the sample topography and the surface potential of AuNPs with $A\beta_{25–35}$ fibrils. From the KPFM images, it was found that the CPD values of the AuNPs are about −0.7 to −1.1 V, whereas the value for pure $A\beta_{25–35}$ peptide fibrils was about 4.62 eV. *Via* calibration of the work function of cantilever tip, the work function of the AuNPs is obtained as about 4.95–5.20 eV. The work functions of fibrils connected by AuNPs are about 4.78 eV, slightly different from the pure fibrils, which difference may be induced by the local electric fields modified by the presence of AuNPs. From the results, it can be suggested that the presence of AuNPs in $A\beta_{25–35}$ solution has a significant influence on protein aggregation and on their electrical properties. This report demonstrated that it is plausible to suggest that KPFM will be quite useful for monitoring the conformational change and the electrical properties of the amyloid fibrils during self-assembly with nanomaterials.

To precisely investigate the mechanism of amyloid fibril formation, it is necessary to quantify the electrical properties of amyloid fibrils synthesized at different chemical environments. In the fibrillation of amyloid fibrils, the pH condition is one of the most important regulating chemical factors. It has been reported that the surface potential distribution of β-lg fibril is variable as a function of the pH of a buffer solution [20]. As mentioned above, the surface potential of amyloid fibril is critically dependent on the conformation of amyloid fibril. Therefore, the authors have defined the point charge density as related to the surface potential of β-lg fibril per unit fibril thickness: $\alpha(x) \equiv \sigma_{\max(x)}/d_{\max(x)}$, where $\sigma(x)$ is the measured surface potential and $d(x)$ is the diameter of an amyloid fibril [20]. It is shown that a parameter $\alpha(x)$ is varied with respect to pH and that $\alpha(x)$ becomes zero at pH ~ 4.7, indicating that the p*I* value of β-lg fibril is given by p*I* = 4.7 (**Figure 11a**). The surface potential of amyloid fibrils ranged from 12 mV (pH ~ 2) to −12 mV (pH ~ 7), depending on the pH of the buffer solution. For precise observation of the β-lg fibril's structure, the authors presented high-resolution KPFM images of single amyloid fibril for pH 3 < p*I* (~5.0) and pH 6 > p*I* (**Figure 11b**). With pH 3, they have found pristine β-lg protofilaments; with pH 6, the β-lg fibril had a complex structure of β-lg oligomer-binding protofilaments that had irregular topological height. It was remarkably observed that the pH-dependent electrostatic property of amyloid fibril was responsible for binding affinity between the amyloid small aggregates and the amyloid fibrils.

http://dx.doi.org/10.5772/63316

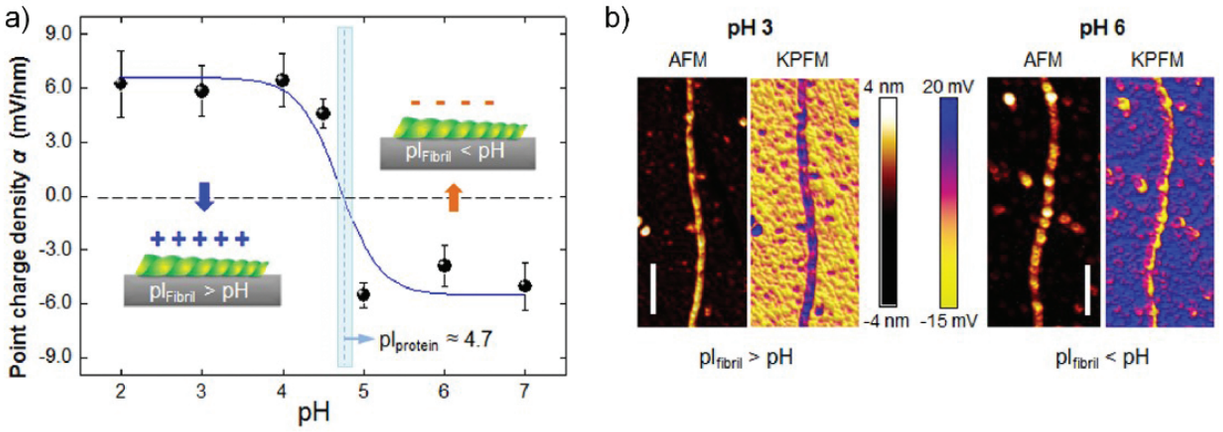


**Figure 11.** (a) The surface charge distribution of amyloid fibril as a function of the pH of buffer solution in which amyloid fibril is prepared. The isoelectric point (p*I*) value of amyloid fibril is determined in such a way that the pH value, at which surface charge distribution becomes zero, is identical to p*I* value. (b) AFM topography and surface potential images of β-lg amyloid fibrils when they are prepared in buffer solutions, whose pH values are pH 3 and pH 6, respectively. All scale bars are 250 nm. Figures reproduced with permission from Ref. [20], © 2012 AIP.

Moreover, in recent studies of amyloid fibril with AFM, some of scientists have reported about various structural features of amyloid fibrils such as steric zipper pattern [76, 77], helical pattern [48], and length [78], which is a key design parameter that determines the material properties of amyloid fibrils. Nevertheless, it is not quite understood yet how the molecular structures and conformational diversity (heterogeneous conformations) of amyloid fibrils are regulated.

To figure out how amyloid fibrils with heterogeneous conformations are formed, the synthesis of the β-lg fibrils with microwave-assisted chemistry method is considered, which enables the acceleration of biochemical reactions, and performed KPFM analysis of them [63]. It has been reported already that the microwave-assisted chemistry for the synthesis of amyloid fibrils makes the acceleration of fibrillation possible. The mechanism of amyloid fibrillation under microwave irradiation is still debated, but it seems to be related to the enhanced collision frequency due to the microwave-driven temperature changes of the protein solution. The temperature of the β-lg protein solution is rapidly increased by rotating water molecules through microwave irradiation. As such, microwave-assisted chemistry accelerates speed of chemical reactions regarding fibrillations of the β-lg proteins within a few hours (even less than an hour) [79]. It is a remarkable result compared to the classical (conventional) heating method which generally requires long incubation time (several hours) and a large volume of protein solution. However the results of this study show that microwave-assisted chemistry not only allows the acceleration of fibrillation but also enables tuning of the β-lg amyloid fibrils by controlling the microwave irradiation time $\tau$, the time interval for irradiation $\lambda$, or the number of irradiations $N$. It was remarkably observed that a stable protein aggregation is produced in the fibril structure that depends on $\lambda$.

**Figure 12** represents the topographic and surface potential images of amyloid fibrils that were synthesized based on microwave-assisted chemistry and their conformational heterogeneities. From these results, it is obvious that except for $\lambda = 60$ s, the surface potential and the fibril

diameter of β-lg amyloid fibrils increase in monotone fashion as $\lambda$ increases. This result revealed that heterogeneous conformations of β-lg amyloid fibrils are due to the wave-driven change of electrostatic interaction, which has a critical impact on the radial growth mechanisms of amyloid fibrils. As described above, KPFM indeed was a good analytical tool for monitoring the conformational change and the electrical properties of amyloid fibrils with respect to microwave-assisted chemistry.

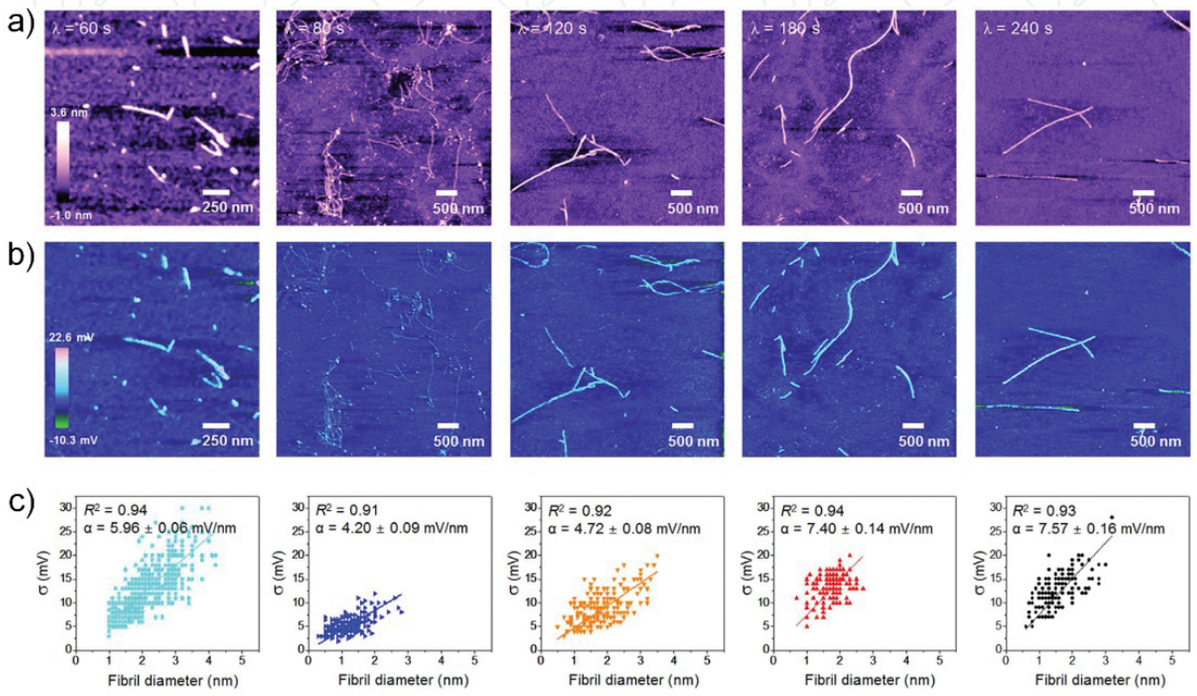


**Figure 12.** (a) AFM images of amyloid fibrils that are synthesized based on microwave-assisted chemistry using different $\lambda$ values. (b) KPFM images of the fibrils formed using different $\lambda$ values. (c) Distribution of surface charges for amyloid fibril as a function of its diameter. The surface potential of an amyloid fibril is almost linearly proportional to its diameter. Figures reprinted with permission from Ref. [63], © 2015 NPG.

## 5. Conclusion and perspectives

As we surveyed above, because of the marvelous capabilities of the conventional AFM device, it and its extensions as liquid AFM, PeakForce QNM, and KPFM have been widely used to perform accurate measurements of mechanical, electrical, and biophysical properties of various amyloid fibrils. AFM applications can provide researchers with the strong advantage of being able to measure the surface potentials of nanomaterials at the single-molecule level. Moreover, it has been demonstrated that AFM applications enable monitoring the fibrillation behavior of various proteins by measuring morphological properties of amyloid fibrils in air or liquid environments. The changes in morphology of the fibrils indicated that amyloid fibrils can be changed morphologically in liquid environments (e.g., human body) and that implies amyloid fibrils would interact differently with other biomolecules, cells, and

tissues in human body. Liquid AFM enables measurement of the characteristics of amyloid fibrils in situ by monitoring the fibrillation and conformation changes of amyloid fibrils. Furthermore, AFM application techniques usually require no labeling with chemical dyes and no chemical reagents for improving the image quality or contrast. Accordingly, AFM is able to get high-resolution images of amyloid fibrils for the detection of conformational changes, by topological imaging in air and liquid environments. We dealt with PeakForce QNM that can simultaneously measure several mechanical properties of amyloid fibrils such as Young's modulus, deformation, and adhesion force by using a precisely operating oscillating probe. With a Kelvin probe, KPFM is highly important for imaging and characterizing the electrical properties (i.e., surface potential and surface potential density of amyloid fibrils) while getting high-resolution topological imaging. Because of these advantages, AFM application is expected to attract much attention as an analytical tool for amyloid research in the future. These AFM-related results shed light on understanding the fibrillation of amyloidogenic proteins and will be the cornerstone for the development of not only the effective prevention methods for amyloidogenic diseases but also therapeutic agents and drugs. These approaches could also contribute to the development of amyloid fibril-based functional nanomaterials such as biocompatible adhesives [80, 81], solar-cell devices [82], and gene delivery systems [83].

## Author details

Wonseok Lee[1], Hyungbeen Lee[1], Gyudo Lee[2] and Dae Sung Yoon[3*]

*Address all correspondence to: dsyoon@korea.ac.kr

1 Department of Biomedical Engineering, Yonsei University, Wonju, Korea

2 School of Public Health, Harvard University, Boston, Massachusetts, USA

3 Department of Bio-convergence Engineering, Korea University, Seoul, Korea

## References

[1] Chiti F, Dobson CM. Protein misfolding, functional amyloid, and human disease. Annu Rev Biochem. 2006;75(1):333–66.

[2] Dobson CM. Protein misfolding, evolution and disease. Trends Biochem Sci. 1999;24(9): 329–32.

[3] Dobson CM. Protein folding and misfolding. Nature. 2003;426(6968):884–90.

[4] Merlini G, Bellotti V. Molecular mechanisms of amyloidosis. N Engl J Med. 2003;349(6): 583–96.

[5] Selkoe DJ. Folding proteins in fatal ways. Nature. 2003;426(6968):900–4.

[6] Fowler DM, Koulov AV, Balch WE, Kelly JW. Functional amyloid – from bacteria to humans. Trends Biochem Sci. 2007;32(5):217–24.

[7] Fowler DM, Koulov AV, Alory-Jost C, Marks MS, Balch WE, Kelly JW. Functional amyloid formation within mammalian tissue. PLoS Biol. 2005;4(1):e6.

[8] Maji SK, Perrin MH, Sawaya MR, Jessberger S, Vadodaria K, Rissman RA, et al. Functional amyloids as natural storage of peptide hormones in pituitary secretory granules. Science. 2009;325(5938):328–32.

[9] Kelly JW, Balch WE. Amyloid as a natural product. J Cell Biol. 2003;161(3):461–2.

[10] Chapman MR, Robinson LS, Pinkner JS, Roth R, Heuser J, Hammar M, et al. Role of Escherichia coli curli operons in directing amyloid fiber formation. Science. 2002;295(5556):851–5.

[11] Shorter J, Lindquist S. Prions as adaptive conduits of memory and inheritance. Nat Rev Genet. 2005;6(6):435–50.

[12] Jung J-M, Savin G, Pouzot M, Schmitt C, Mezzenga R. Structure of heat-induced β-lactoglobulin aggregates and their complexes with sodium-dodecyl sulfate. Biomacromolecules. 2008;9(9):2477–86.

[13] Knowles TPJ, Buehler MJ. Nanomechanics of functional and pathological amyloid materials. Nat Nanotechnol. 2011;6(8):469–79.

[14] Rubin N, Perugia E, Goldschmidt M, Fridkin M, Addadi L. Chirality of amyloid suprastructures. J Am Chem Soc. 2008;130(14):4602–3.

[15] Kowalewski T, Holtzman DM. In situ atomic force microscopy study of Alzheimer's β-amyloid peptide on different substrates: new insights into mechanism of β-sheet formation. Proc Natl Acad Sci. 1999;96(7):3688–93.

[16] Jeong JS, Ansaloni A, Mezzenga R, Lashuel HA, Dietler G. Novel mechanistic insight into the molecular basis of amyloid polymorphism and secondary nucleation during amyloid formation. J Mol Biol. 2013;425(10):1765–81.

[17] Adamcik J, Berquand A, Mezzenga R. Single-step direct measurement of amyloid fibrils stiffness by peak force quantitative nanomechanical atomic force microscopy. Appl Phys Lett. 2011;98(19):193701.

[18] Sweers K, van der Werf K, Bennink M, Subramaniam V. Nanomechanical properties of α-synuclein amyloid fibrils: a comparative study by nanoindentation, harmonic force microscopy, and Peakforce QNM. Nanoscale Res Lett. 2011;6(1):1–10.

[19] Adamcik J, Lara C, Usov I, Jeong JS, Ruggeri FS, Dietler G, et al. Measurement of intrinsic properties of amyloid fibrils by the peak force QNM method. Nanoscale. 2012;4(15):4426–9.

[20] Lee G, Lee W, Lee H, Lee SW, Yoon DS, Eom K, et al. Mapping the surface charge distribution of amyloid fibril. Appl Phys Lett. 2012;101(4):043703–4.

[21] Ruggeri FS, Adamcik J, Jeong JS, Lashuel HA, Mezzenga R, Dietler G. Influence of the β-sheet content on the mechanical properties of aggregates during amyloid fibrillization. Angew Chem Int Ed. 2015;54(8):2462–6.

[22] Lamour G, Yip CK, Li H, Gsponer J. High intrinsic mechanical flexibility of mouse prion nanofibrils revealed by measurements of axial and radial Young's moduli. ACS Nano. 2014;8(4):3851–61.

[23] Lee W, Jung H, Son M, Lee H, Kwak TJ, Lee G, et al. Characterization of the regrowth behavior of amyloid-like fragmented fibrils decomposed by ultrasonic treatment. RSC Adv 2014;4(100):56561–6.

[24] Jaroniec CP, MacPhee CE, Bajaj VS, McMahon MT, Dobson CM, Griffin RG. High-resolution molecular structure of a peptide in an amyloid fibril determined by magic angle spinning NMR spectroscopy. Proc Natl Acad Sci U S A. 2004;101(3):711–6.

[25] Meersman F, Cabrera RQ, McMillan PF, Dmitriev V. Compressibility of insulin amyloid fibrils determined by X-ray diffraction in a diamond anvil cell. High Pressure Res. 2009;29(4):665–70.

[26] Westermark P, Benson MD, Buxbaum JN, Cohen AS, Frangione B, Ikeda S, et al. Amyloid fibril protein nomenclature—2002. Amyloid. 2002;9(3):197.

[27] Khurana R, Coleman C, Ionescu-Zanetti C, Carter SA, Krishna V, Grover RK, et al. Mechanism of thioflavin T binding to amyloid fibrils. J Struct Biol. 2005;151(3):229–38.

[28] Giessibl FJ. Advances in atomic force microscopy. Rev Mod Phys. 2003;75(3):949.

[29] Binnig G, Quate CF, Gerber C. Atomic force microscope. Phys Rev Lett. 1986;56(9):930.

[30] Muller DJ, Dufrene YF. Atomic force microscopy as a multifunctional molecular toolbox in nanobiotechnology. Nat Nanotechnol. 2008;3(5):261–9.

[31] Custance O, Perez R, Morita S. Atomic force microscopy as a tool for atom manipulation. Nat Nanotechnol. 2009;4(12):803–10.

[32] Nam K, Lee G, Jung H, Park J, Kim CH, Seo J, et al. Single-step electropolymerization patterning of a polypyrrole nanowire by ultra-short pulses via an AFM cantilever. Nanotechnology. 2011;22(22):225303.

[33] Lee G, Jung H, Son J, Nam K, Kwon T, Lee G, et al. Experimental and numerical study of electrochemical nanomachining using an AFM cantilever tip. Nanotechnology. 2010;21(18):185301.

[34] Khurana R, Ionescu-Zanetti C, Pope M, Li J, Nielson L, Ramírez-Alvarado M, et al. A general model for amyloid fibril assembly based on morphological studies using atomic force microscopy. Biophys J. 2003;85(2):1135–44.

[35] Adamcik J, Jung J-M, Flakowski J, De Los Rios P, Dietler G, Mezzenga R. Understanding amyloid aggregation by statistical analysis of atomic force microscopy images. Nat Nanotechnol. 2010;5(6):423–8.

[36] Sagis LMC, Veerman C, van der Linden E. Mesoscopic properties of semiflexible amyloid fibrils. Langmuir. 2004;20(3):924–7.

[37] Bolisetty S, Adamcik J, Mezzenga R. Snapshots of fibrillation and aggregation kinetics in multistranded amyloid [small beta]-lactoglobulin fibrils. Soft Matter. 2011;7(2): 493–9.

[38] Relini A, Rolandi R, Bolognesi M, Aboudan M, Merlini G, Bellotti V, et al. Ultrastructural organization of ex vivo amyloid fibrils formed by the apolipoprotein A-I Leu174Ser variant: an atomic force microscopy study. Biochim Biophys Acta. 2004;1690(1):33–41.

[39] Sweers KKM, van der Werf KO, Bennink ML, Subramaniam V. Atomic force microscopy under controlled conditions reveals structure of C-terminal region of $\alpha$-synuclein in amyloid fibrils. ACS Nano. 2012;6(7):5952–60.

[40] Ahmed M, Davis J, Aucoin D, Sato T, Ahuja S, Aimoto S, et al. Structural conversion of neurotoxic amyloid-[beta]1–42 oligomers to fibrils. Nat Struct Mol Biol. 2010;17(5):561–7.

[41] Cherny I, Gazit E. Amyloids: not only pathological agents but also ordered nanomaterials. Angew Chem Int Ed. 2008;47(22):4062–9.

[42] Smith JF, Knowles TPJ, Dobson CM, MacPhee CE, Welland ME. Characterization of the nanoscale properties of individual amyloid fibrils. Proc Natl Acad Sci. 2006;103(43): 15806–11.

[43] Pfreundschuh M, Martinez-Martin D, Mulvihill E, Wegmann S, Muller DJ. Multiparametric high-resolution imaging of native proteins by force-distance curve-based AFM. Nat Protoc. 2014;9(5):1113–30.

[44] Ferencz R, Sanchez J, Blümich B, Herrmann W. AFM nanoindentation to determine Young's modulus for different EPDM elastomers. Polym Test. 2012;31(3):425–32.

[45] Foster B. New atomic force microscopy (AFM) approaches life sciences gently, quantitatively, and correlatively. Am Lab 2012(4):24–8.

[46] Trtik P, Kaufmann J, Volz U. On the use of peak-force tapping atomic force microscopy for quantification of the local elastic modulus in hardened cement paste. Cem Concr Res. 2012;42(1):215–21.

[47] Lee G, Lee H, Nam K, Han J-H, Yang J, Lee SW, et al. Nanomechanical characterization of chemical interaction between gold nanoparticles and chemical functional groups. Nanoscale Res Lett. 2012;7(1):1–11.

[48] Knowles TP, Fitzpatrick AW, Meehan S, Mott HR, Vendruscolo M, Dobson CM, et al. Role of intermolecular forces in defining material properties of protein nanofibrils. Science. 2007;318(5858):1900–3.

[49] Strohman R. Maneuvering in the complex path from genotype to phenotype. Science. 2002;296(5568):701–3.

[50] Verdile G, Fuller S, Atwood CS, Laws SM, Gandy SE, Martins RN. The role of beta amyloid in Alzheimer's disease: still a cause of everything or the only one who got caught? Pharmacol Res. 2004;50(4):397–409.

[51] Drolle E, Hane F, Lee B, Leonenko Z. Atomic force microscopy to study molecular mechanisms of amyloid fibril formation and toxicity in Alzheimer's disease. Drug Metab Rev. 2014;46(2):207–23.

[52] Bucciantini M, Giannoni E, Chiti F, Baroni F, Formigli L, Zurdo J, et al. Inherent toxicity of aggregates implies a common mechanism for protein misfolding diseases. Nature. 2002;416(6880):507–11.

[53] Kayed R, Head E, Thompson JL, McIntire TM, Milton SC, Cotman CW, et al. Common structure of soluble amyloid oligomers implies common mechanism of pathogenesis. Science. 2003;300(5618):486–9.

[54] Glabe CG, Kayed R. Common structure and toxic function of amyloid oligomers implies a common mechanism of pathogenesis. Neurology. 2006;66(1 suppl 1):S74–S8.

[55] Hertel C, Terzi E, Hauser N, Jakob-Røtne R, Seelig J, Kemp J. Inhibition of the electrostatic interaction between β-amyloid peptide and membranes prevents β-amyloid-induced toxicity. Proc Natl Acad Sci. 1997;94(17):9412–6.

[56] Bokvist M, Lindström F, Watts A, Gröbner G. Two types of Alzheimer's β-amyloid (1–40) peptide membrane interactions: aggregation preventing transmembrane anchoring versus accelerated surface fibril formation. J Mol Biol. 2004;335(4):1039–49.

[57] Friedman R, Pellarin R, Caflisch A. Amyloid aggregation on lipid bilayers and its impact on membrane permeability. J Mol Biol. 2009;387(2):407–15.

[58] Nonnenmacher M, o'Boyle M, Wickramasinghe H. Kelvin probe force microscopy. Appl Phys Lett. 1991;58(25):2921–3.

[59] Sinensky AK, Belcher AM. Label-free and high-resolution protein/DNA nanoarray analysis using Kelvin probe force microscopy nature nanotechnology. Nat Nanotechnol. 2007;2(10):653–9.

[60] Leung C, Maradan D, Kramer A, Howorka S, Mesquida P, Hoogenboom BW. Improved Kelvin probe force microscopy for imaging individual DNA molecules on insulating surfaces. Appl Phys Lett. 2010;97(20):203703.

[61] Park J, Yang J, Lee G, Lee CY, Na S, Lee SW, et al. Single-molecule recognition of biomolecular interaction via Kelvin probe force microscopy. ACS Nano. 2011;5(9): 6981–90.

[62] Nam K, Eom K, Yang J, Park J, Lee G, Jang K, et al. Aptamer-functionalized nanopattern based on carbon nanotube for sensitive, selective protein detection. J Mater Chem. 2012;22(44):23348–56.

[63] Lee G, Lee W, Lee H, Lee CY, Eom K, Kwon T. Self-assembled amyloid fibrils with controllable conformational heterogeneity. Sci Rep 2015;5.

[64] Gao P, Cai Y. Label-free detection of the aptamer binding on protein patterns using Kelvin probe force microscopy (KPFM). Anal Bioanal Chem. 2009;394(1):207–14.

[65] Kelvin LV. Contact electricity of metals. Philos Mag 1898;46(278):82–120.

[66] Melitz W, Shen J, Kummel AC, Lee S. Kelvin probe force microscopy and its application. Surf Sci Rep. 2011;66(1):1–27.

[67] Ma Q, Wei G, Yang X. Influence of Au nanoparticles on the aggregation of amyloid-β-(25–35) peptides. Nanoscale. 2013;5(21):10397–403.

[68] Choi JH, Nguyen FT, Barone PW, Heller DA, Moll AE, Patel D, et al. Multimodal biomedical imaging with asymmetric single-walled carbon nanotube/iron oxide nanoparticle complexes. Nano Lett. 2007;7(4):861–7.

[69] McCarthy JR, Jaffer FA, Weissleder R. A macrophage-targeted theranostic nanoparticle for biomedical applications. Small. 2006;2(8-9):983–7.

[70] Kelley SO, Mirkin CA, Walt DR, Ismagilov RF, Toner M, Sargent EH. Advancing the speed, sensitivity and accuracy of biomolecular detection using multi-length-scale engineering. Nat Nanotechnol. 2014;9(12):969–80.

[71] Lin Y-C, Yu B-Y, Lin W-C, Lee S-H, Kuo C-H, Shyue J-J. Tailoring the surface potential of gold nanoparticles with self-assembled monolayers with mixed functional groups. J Colloid Interface Sci. 2009;340(1):126–30.

[72] Conklin D, Nanayakkara S, Park T-H, Lagadec MF, Stecher JT, Therien MJ, et al. Electronic transport in porphyrin supermolecule-gold nanoparticle assemblies. Nano Lett. 2012;12(5):2414–9.

[73] Stehlik S, Petit T, Girard HA, Kromka A, Arnault J-C, Rezek B. Surface potential of diamond and gold nanoparticles can be locally switched by surrounding materials or applied voltage. J Nanopart Res. 2014;16(4):1–11.

[74] Gutiérrez-Sánchez C, Pita M, Vaz-Domínguez C, Shleev S, De Lacey AL. Gold nanoparticles as electronic bridges for laccase-based biocathodes. J Am Chem Soc. 2012;134(41):17212–20.

[75] Raschke G, Kowarik S, Franzl T, Sönnichsen C, Klar T, Feldmann J, et al. Biomolecular recognition based on single gold nanoparticle light scattering. Nano Lett. 2003;3(7): 935–8.

[76] Yoon G, Lee M, Kim JI, Na S, Eom K. Role of sequence and structural polymorphism on the mechanical properties of amyloid fibrils. PLoS one. 2014;9(2):e88502.

[77] Sawaya MR, Sambashivan S, Nelson R, Ivanova MI, Sievers SA, Apostol MI, et al. Atomic structures of amyloid cross-β spines reveal varied steric zippers. Nature. 2007;447(7143):453–7.

[78] Choi B, Yoon G, Lee SW, Eom K. Mechanical deformation mechanisms and properties of amyloid fibrils. Phys Chem Chem Phys. 2015;17(2):1379–89.

[79] Hettiarachchi CA, Melton LD, Gerrard JA, Loveday SM. Formation of β-lactoglobulin nanofibrils by microwave heating gives a peptide composition different from conventional heating. Biomacromolecules. 2012;13(9):2868–80.

[80] Mankar S, Anoop A, Sen S, Maji SK. Nanomaterials: amyloids reflect their brighter side. Nano Rev 2011;2.

[81] Mostaert AS, Higgins MJ, Fukuma T, Rindi F, Jarvis SP. Nanoscale mechanical characterisation of amyloid fibrils discovered in a natural adhesive. J Biol Phys. 2006;32(5):393–401.

[82] Bolisetty S, Adamcik J, Heier J, Mezzenga R. Amyloid directed synthesis of titanium dioxide nanowires and their applications in hybrid photovoltaic devices. Adv Funct Mater. 2012;22(16):3424–28.

[83] Yolamanova M, Meier C, Shaytan AK, Vas V, Bertoncini CW, Arnold F, et al. Peptide nanofibrils boost retroviral gene transfer and provide a rapid means for concentrating viruses. Nat Nanotechnol. 2013;8(2):130–6.

IntechOpen